JOURNAL OF AIRCRAFT
Vol. 47, No. 2, March–April 2010

Prediction of Ballistic Separation Effect by Direct Calculation of Incremental Coefficients

Eugene Kim* and Jang Hyuk Kwon†
Korea Advanced Institute of Science and Technology, Daejon 305-701, Republic of Korea
and
Soo Hyung Park‡
Konkuk University, Seoul 143-701, Republic of Korea

DOI: 10.2514/1.45915

The ballistic separation effect in an aircraft flowfield was predicted via the direct calculation of incremental coefficients. A highly robust flow solver, including a Chimera grid module, was used to create the trajectory of a released store and to calculate incremental coefficients. The incremental coefficients were computed according to the difference between the aerodynamic coefficients in the aircraft flowfield and in the freestream condition. Two different calculations can be executed simultaneously in a parallel computing environment. The aircraft flowfield effect was measured using the incremental coefficients. This method of direct calculation of the incremental coefficients was tested in the case of released stores in two-dimensional subsonic and supersonic flow regions. The accuracy of the unsteady trajectory calculation was verified through comparisons with the captive trajectory system data in the Eglin wing/pylon/store separation problem. The method was then applied to a generic bomb released from a full-body aircraft. The computational results show that the current method is capable of simulating the store trajectory and investigating aircraft flowfield effects.

Nomenclature

C_l, C_m, C_n	=	store rolling, pitching, and yawing moment coefficients
C_{mx}	=	moment coefficient in the x direction
C_x	=	force coefficient in the x direction
dx	=	displacement in the x direction
$\mathbf{F}_i$	=	generalized flux vector
H	=	total enthalpy
M_∞	=	freestream Mach number
n	=	outward normal vector
$\mathbf{Q}$	=	conservative flow variables
t	=	time
U, V, W	=	contravariant velocities along the generalized coordinates
U_g	=	grid velocity
u, v, w	=	Cartesian velocity components
ΔC_x	=	incremental force coefficient in the x direction
ρ, p, e	=	density, pressure, and total energy
Φ, Ψ, Θ	=	roll, yaw, and pitch angles

I. Introduction

TARGET point estimation is an important objective in flight tests, as well as safe separation, when weapons are integrated on an aircraft. The impact point of an unguided bomb without control surfaces is determined by firing input from the pilot. As a result, bomb release and impact predictions are important. The bombing function of the aircraft fire control computes the target point and presents the data to the position on a heads-up display in real time. The computational algorithm must be as simple as possible. The store in the bombing function is represented as a point–mass particle located at its center of gravity. Drag force and gravity act upon this element as the computer runs a simulation during every computational cycle (0.02–0.25 s) [1,2].

The dynamics of a released bomb are much more complicated than predicted by an aircraft fire control computer. The actual trajectory is perturbed by aircraft separation effects, including ejector-induced forces and moments, and by the aircraft flowfield effects. The latter, known as the ballistic separation effect (BSE), is one of the largest miss-distance factors. Moreover, it is difficult to predict correctly. The operational flight program of an aircraft must account for the BSE and make appropriate corrections by modifying the initial conditions to a three-degree-of-freedom (DOF) predictor [2,3]. Therefore, an accurate trajectory to the target point is required to model the bombing function.

The best approach for generating a trajectory is a flight test under realistic conditions, including atmospheric situations and wing deformations, although the safety risks and the expense involved in gaining dynamic data are considerable. Other approaches, such as wind-tunnel testing [captive trajectory system (CTS) and free drop] and different prediction methods generate a trajectory model or help design a flight-test schedule [4]. Engineering-level methods [5] and semiempirical methods, such as the grid method [6] and the influence function method [7], have also been applied to generate the trajectory.

The time-accurate computational fluid dynamics (CFD) technique is often used to predict store separation events [8–11]. The CHIMERA scheme [12] is ideally suited to perform calculations with moving bodies. The calculation of the aerodynamic load is fully coupled with the dynamics of the released bomb. This technique is commonly applied to short-range predictions after separation due to its high computing cost [9–11]. Recent advances in computing environments have increased the reliance of CFD methods to simulate store separations. A steady flowfield database with the CFD method substitutes for wind-tunnel data in the trajectory generation program (TGP) [13].

The general TGP uses a database that is a superposition of freestream aerodynamic loads and incremental coefficients [4]. The interference database is usually generated by a wind-tunnel test. The advantage of using a database is the capability to generate numerous

Received 11 June 2009; revision received 19 December 2009; accepted for publication 21 December 2009.

*Doctoral Candidate, Department of Aerospace Engineering, 373-1 Guseong-dong, Yuseong-gu.
†Professor, Department of Aerospace Engineering, 373-1 Guseong-dong, Yuseong-gu; jhkwon@kaist.ac.kr. Senior Member AIAA.
‡Assistant Professor, Department of Aerospace Information Engineering, 1 Hwayang-dong, Gwangjin-Gu; pish@konkuk.ac.kr. Member AIAA.

trajectories with one set. However, this database is mostly static data with interpolation errors.

Incremental aerodynamic coefficients in an aircraft flowfield are calculated directly with the CFD approach. The elimination of these coefficients is checked simultaneously for the indicator of aircraft flowfield effect in the current process. A subprogram is executed with another grid system in the freestream condition with the same dynamics, while an unsteady calculation is done to generate the trajectory of the released store. Time-accurate grid velocities are applied to the subcalculation, whereas only the rotation is updated for the Euler angles of the store, because altitude effects are neglected in this simulation. The store is considered out of the aircraft flowfield if the incremental coefficients converge to zero. A simple TGP algorithm with a freestream database is executed to trace target points using the dynamics in that time as an initial condition. The TGP algorithm has two steps: the first for the BSE region and the second for the free-flight region. The former case is described and applied in this paper to calculate the BSE in aircraft flowfields.

A flow solver, including a parallelized grid assembly, was developed and used for the unsteady calculation [14]. Two-dimensional supersonic and subsonic store separation cases were simulated, and incremental coefficients were computed to assess the suitability of the developed algorithms. An ejected bomb case from an Eglin wing and a pylon configuration in a transonic flowfield were tested to validate the generated trajectory. Unsteady trajectory generation in an aircraft flowfield and direct calculation of the incremental coefficients were applied to the released generic bomb cases from a Korean basic training aircraft, the KT-1, and the aircraft flowfields were estimated for a number of separation scenarios.

II. Numerical Methods

A. Flow Solver

The three-dimensional compressible Euler equations were written in integral form over the control volume $V(t)$:

$$\frac{\mathrm{d}}{\mathrm{d}t}\int_{V(t)} Q\,\mathrm{d}V + \int_{\partial V(t)} F\,\mathrm{d}S = 0 \tag{1}$$

where the conservative flow variable $Q = [\rho,\ \rho u,\ \rho v,\ \rho w,\ \rho e]^T$. Frepresents the inviscid fluxes:

$$F = \begin{bmatrix} \rho U \\ \rho u U + n_x p \\ \rho v U + n_y p \\ \rho w U + n_z p \\ \rho H U + p U_g \end{bmatrix} \tag{2}$$

Here, ρ and p are the density and the pressure. The total energy is e, and $H = e + p/\rho$ is the total enthalpy.

U is the relative flow velocity on the cell face in each direction, and U_g is the moving velocity of the control volume:

$$U = n_x u + n_y v + n_z w - U_g \tag{3}$$

This system was discretized using a finite volume method. Numerical flux functions were constructed using the Roe scheme with Harten's fix function [15] for entropy correction. MUSCL reconstruction of primitive variables [16] was applied to obtain higher-order spatial accuracy, whereas the minmod or van Albada's limiter was used to maintain a total-variation-diminishing property near the shocks. The diagonalized alternating-direction-implicit method [17] was used for time integration, and the second-order dual-time-stepping algorithm [18] was used to advance the solution in time. The number of dual-time iterations was approximately 20, which is sufficient for accurate simulations through numerical experiments. The Riemann invariants were used for the boundary condition at the far-field boundary and the flow tangency condition at the body surface. The equations of motion of a moving body were integrated with the four-stage Runge–Kutta method.

B. Parallelized Grid Assembly

The CHIMERA method offers not only efficient grid generation but the capability of handling the relative movement of multiple bodies. However, the information to connect overlapped grids must be reestablished whenever a grid is moved. This process of establishing communication is referred to as a grid assembly [19]. In this paper, the grid assembly was parallelized with static load balancing based on the decomposed grid system of a flow solver. Coarse-grained communication was optimized with minimized memory allocation and a communication load, as the parallel grid assembly

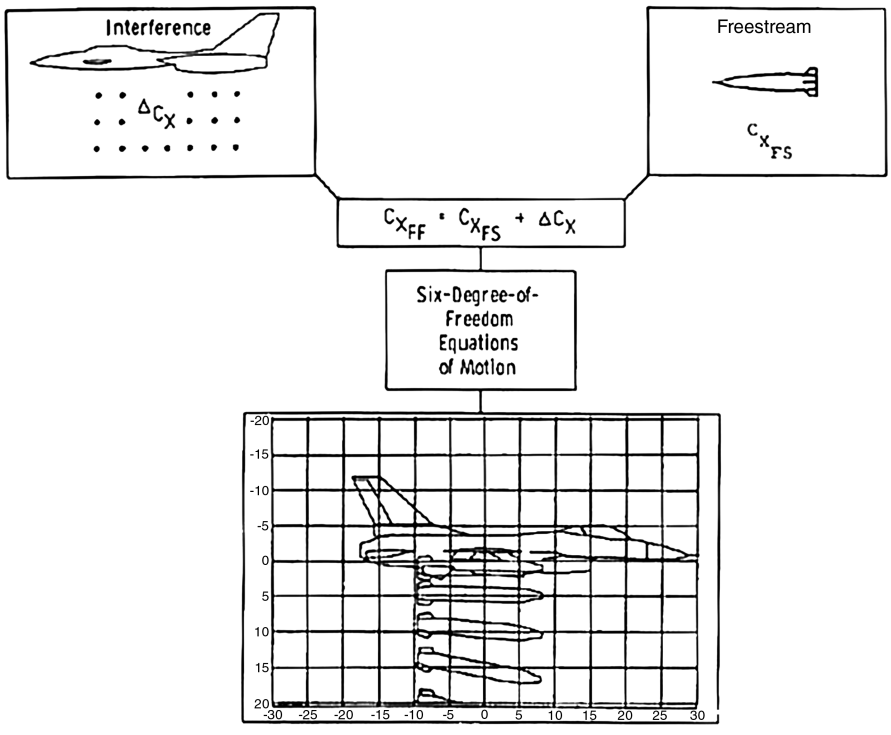

Fig. 1 Schematic of the grid delta-coefficient trajectory method [4].

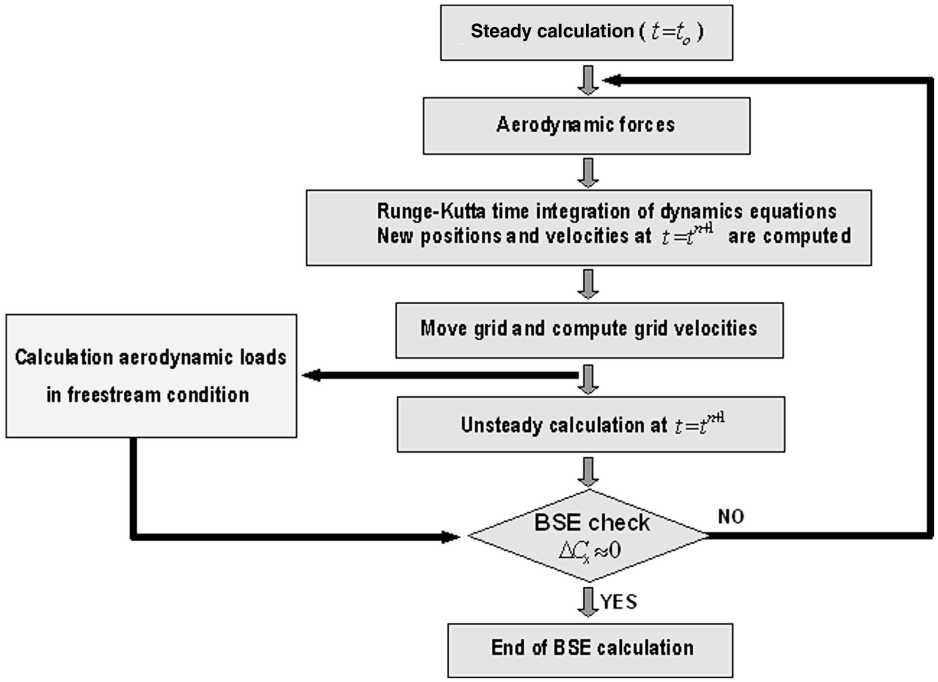

Fig. 2 Direct calculation of incremental coefficients and the BSE region check.

accesses the decomposed geometry data within other processors only by passing messages in a distributed memory system, such as a PC cluster. A parallel performance assessment of a moving body overset grid application on a PC cluster was achieved [14].

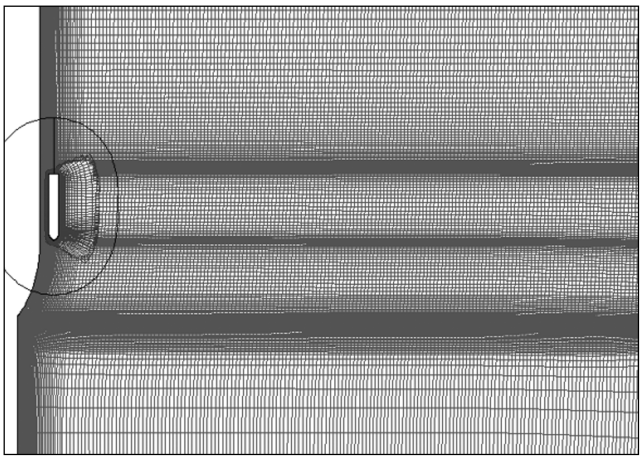

Fig. 3 Initial overset grids: dispensed submunition case.

The overset grid method is composed of two major steps: hole cutting and donor cell identification. Zones of an interference scheme and a hole-map algorithm are used for the hole-cutting procedure. A stencil walk and gradient-searching methods are adapted for the second step [20]. Solid walls are initially used for hole-cutting surfaces, and an automatic cut–paste algorithm [20] is used to construct an optimal mesh interface. The gathering of surface patches in each body is executed by group communication after the regeneration of a new communicator among the processors related to the same body, as only a closed surface is used to make the hole map. Interpolation and donor data in the take and send processors, respectively, are connected by sorting with a tag index. Thus, minimized information of the interpolation points is communicated between the take and send processors during parallel donor searches. A detailed description of the parallelization and performance of the grid assembly is shown in [14].

C. Direct Calculation of Incremental Coefficients

The general trajectory generating process, with superposition of freestream aerodynamic loads and delta coefficients, is shown in Fig. 1 [4]. The interference database was generated from the differences between aerodynamic coefficients in the aircraft flowfield and in the freestream condition. However, these are only static data,

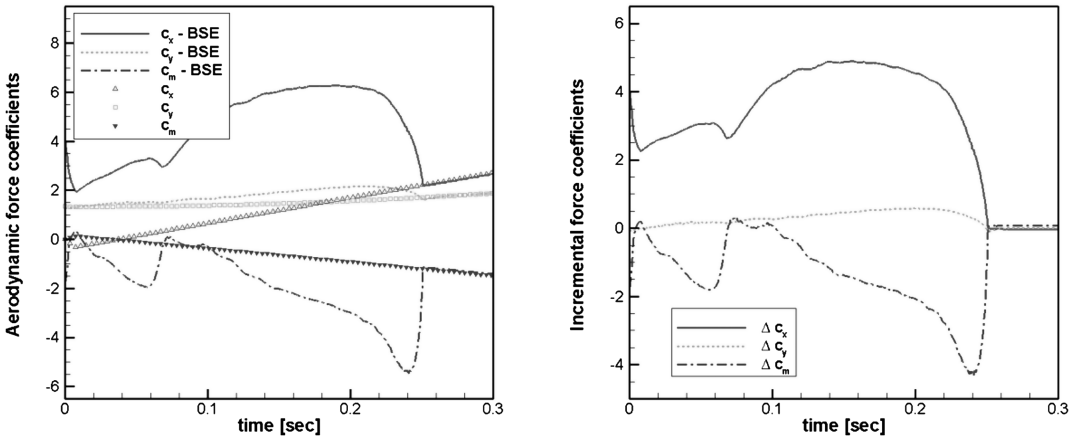

Fig. 4 Aerodynamic forces and incremental coefficients: dispensed submunition, $M_\infty = 1.8$.

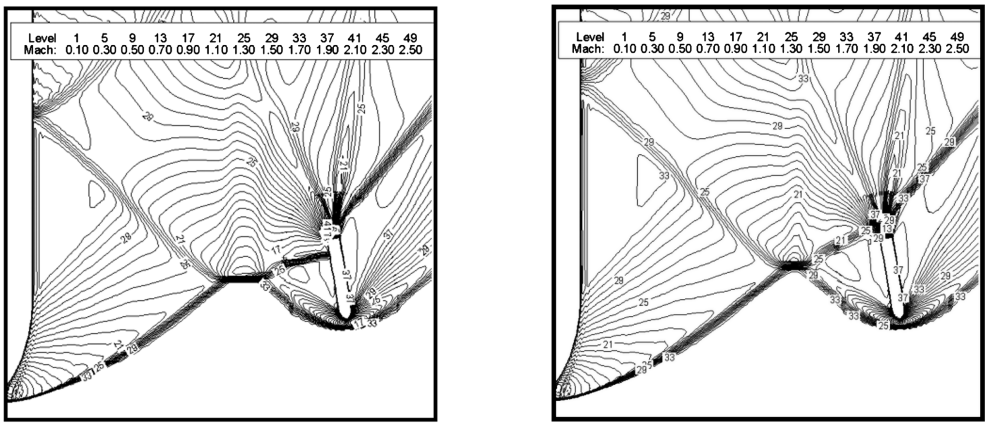

a) t=0.24916 sec. b) t=0.25414 sec.

Fig. 5 Temporal Mach number contours: dispensed submunition, $M_\infty = 1.8$.

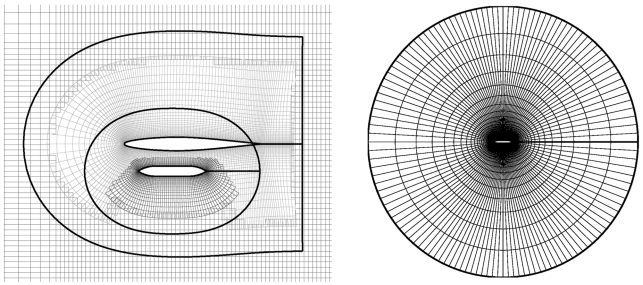

a) Overset grids b) Grid for BSE check

Fig. 6 Grid systems for the case of a store drop from an airfoil.

without considering dynamics of store, and must be interpolated to make force coefficients at the exact store position.

In this study, the incremental aerodynamic coefficients in the BSE regime were computed directly by considering time-accurate dynamics, contrary to the classical procedure (Fig. 1). The elimination of the flowfield effect was simultaneously observed by measuring the magnitude of the incremental coefficients. A flowchart of the algorithm, developed for a direct calculation of the incremental coefficients and to verify the BSE, is shown in Fig. 2. A subprogram was simultaneously executed with another grid system in the freestream condition, while the unsteady computation was achieved to generate the trajectory of the released store. The multiple-program/multiple-data paradigm was applied to this coupled analysis. Time-accurate grid velocities were calculated with 6-DOF motion equations and were applied to the unsteady calculation. These were also applied to the subcalculation in the freestream condition. The aerodynamic forces and the moments of the subcalculation were subtracted from those of the unsteady calculation. The differences are the incremental coefficients in this situation and the aerodynamic forces disturbed by the aircraft flowfield effects.

III. Verification of the Direct Calculation

Two cases of two-dimensional problems were simulated: store separations in supersonic and subsonic flowfields. Incremental coefficients, calculated to investigate the aircraft field effects, were estimated by the present approach. The first case involves a submunition dispensed from a mother missile dropping with a speed of Mach 1.8. The initial overset grids were constructed (Fig. 3) with an O-type grid about the submunition (161 × 25), an H-type grid for the mother missile, and the entire computational domain (184× 210). The internal bay of the mother missile was disregarded in this case, owing to the use of an inviscid calculation. The aerodynamic force coefficients and the incremental coefficients are shown in Fig. 4. BSE in the legend indicates that the result considered the mother missile flowfields, whereas the submunition results in the freestream flowfield are shown in the legend without BSE. Two side-ejecting forces act on the moving body in the short range, and the ejector stroke length is 36% of the diameter of the submunition. The positions are forward and aft of the center of gravity, which creates an initial nose-down moment. Two temporal Mach number contours are shown in Fig. 5. The normal shock wave on the submunition interacted with the shock wave from the mother missile (Fig. 5a). This shock moved suddenly to the aft of the body, and the angle of the oblique shock became large, causing the incremental coefficients to fade out suddenly (Fig. 5b). It is difficult to predict the interaction between the mother missile and the submunition correctly with a

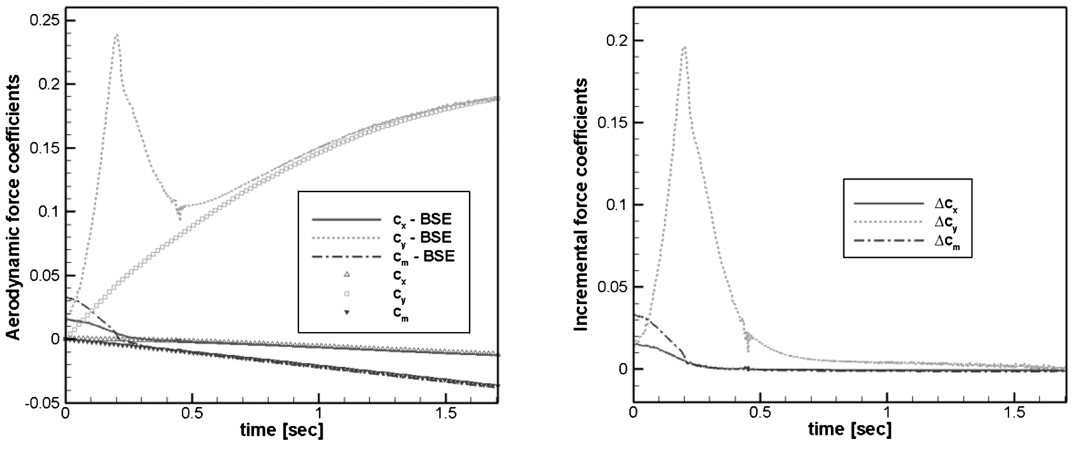

a) b)

Fig. 7 Aerodynamic forces and incremental coefficients: released store, $M_\infty = 0.6$.

Table 1 Grid system for the Eglin wing/pylon/store case

Body	No. of blocks	Grid type	No. of nodes
Wing	1	C–H	$129 \times 44 \times 49$
Pylon	1	C–O	$121 \times 27 \times 26$
Store	4	O–H	$130 \times 32 \times 25$
Background block	1	H–H	$105 \times 51 \times 85$

transonic nonlinear characteristic in transonic regimes, as the flowfield is dominated considerably by shock waves. Furthermore, the flowfield becomes more complicated as the number of submunitions is increased.

Results from wind-tunnel tests or quasi-steady CFD methods cannot capture the transonic nonlinearity of aerodynamic forces and moments. Therefore, costly and time-consuming flight tests continue to be necessary to obtain the trajectory data, especially in the transonic speed range. The unsteady CFD approach, however, provides reliable data with less time and cost in the transonic regime and captures nonlinear phenomena, such as the sudden changes of aerodynamic forces and moment at 0.25 s, shown as Fig. 5.

The second case involves a released store from an airfoil in the subsonic flow regime. The freestream Mach number was 0.6. The store was dropped freely into the stream. The computational domain is decomposed into three different grids: a C-type grid about the airfoil (193×33), an O-type grid (129×25), and an H-type grid (137×419) for the entire computational domain. The background grid was constructed to maintain a fine-grid resolution in the store path. The far-field boundary was extended to eight times the chord length of the store for calculation in the freestream condition (Fig. 6b). The aerodynamic forces and the delta coefficients are

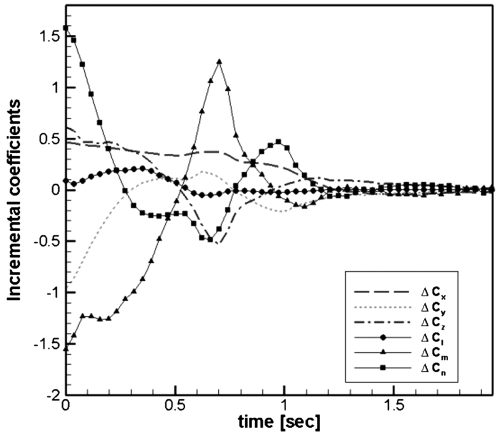

Fig. 10 Incremental coefficients (Eglin wing/pylon/store case).

shown in Fig. 7. A small lifting force remains longer in time than in the case of the supersonic flow calculation. The extended grid used for the computation in the freestream condition makes a difference in the convergence; the minor difference in the incremental lift coefficient was found to be prominent, owing to the relatively small aerodynamic forces and moment when compared with these factors in the supersonic case. However, there is no sudden change of the aerodynamic forces and moments after 0.5 s when compared with the supersonic flow condition. The drag force and pitching moment incremental coefficients converged more rapidly than the lifting force, because there were lower moving grid velocities when compared with those of the released direction.

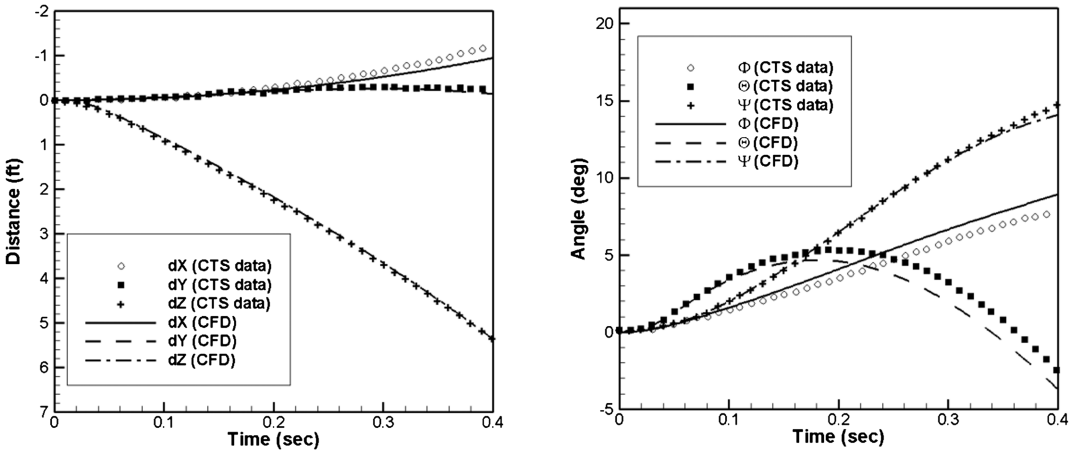

Fig. 8 Displacement and angular trajectory of the ejected store.

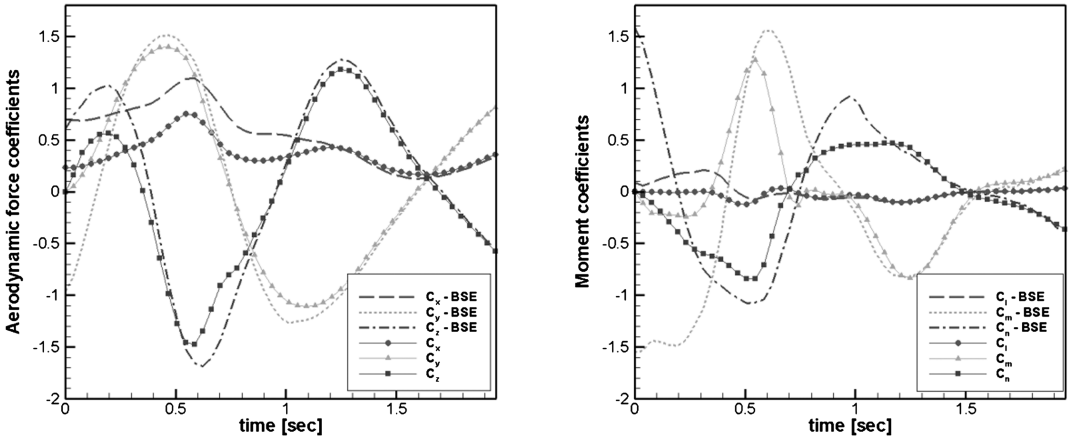

Fig. 9 Aerodynamic force and moment coefficients (Eglin wing/pylon/store case).

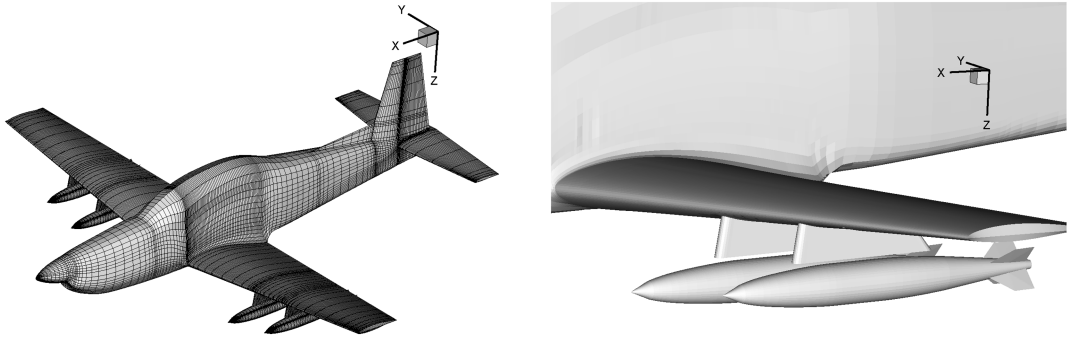

Fig. 11 Surface mesh and initial bomb positions.

IV. Validation

The validity of the direct calculation of incremental coefficients and the solution accuracy were tested against CTS data [9]. The grid system is listed in Table 1. The total number of each grid was approximately one million. The H–H-type background grid was used around the store trajectory, which was sufficient to maintain the interpolation accuracy of overlapped subgrids. The nondimensionalized unsteady time step was set to 2.0, and the dynamics of the store were calculated up to 1.95 s, with 500 time steps marching. The total computing time was nearly 3 h, using 24 processors in a Linux PC cluster consisting of a Pentium 4 2.6 GHz CPU in each node and linked into a 100 Mbps Ethernet network. The linear and angular trajectory results of the ejected store were compared with the CTS data (Fig. 8) and were closely matched to the wind-tunnel data. Similar results were obtained in two earlier studies (see [9,20]).

The elimination of the flowfield effect was observed in measurements of two dominant aerodynamic force coefficients, the lift and the pitching moment, as different grid systems may cause discrepancies in the results and convergence of the force coefficients. Convergence of the incremental coefficients was checked with criteria that indicated whether these coefficients were reduced by an order of 10^{-2} of each peak value. Furthermore, the BSE was considered to be diminished when five successive convergence checks satisfied that criteria, as there was pitch oscillation caused by ejecting systems.

The computed aerodynamic forces of the store, with and without the wing, and are shown in Fig. 9. Incremental force coefficients from the differences in the aerodynamic forces in the two systems were calculated (Fig. 10). Those at initial condition were reduced after 1.5 s and converged to an order of 10^{-2} of each peak value. The computed BSE diminishing time was 1.89 s, whereas the store departed 77 ft below (about three times the root chord length) at that time from the initial position.

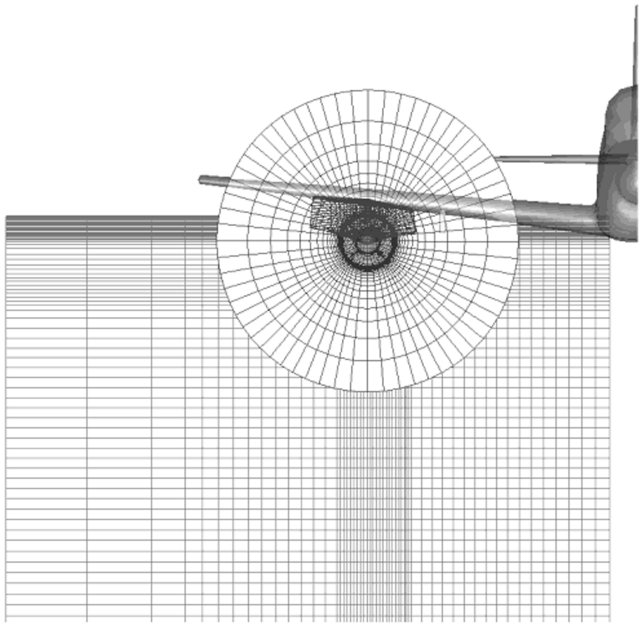

Fig. 12 Grid system: medium set (front view).

V. Application

A generic store separation case from the KT-1 aircraft was tested to estimate the aircraft field effects. The surface mesh and the initial position of the store are shown in Fig. 11. Test cases of store separation from inboard and outboard pylons were simulated. The total grid system consisted of 33 blocks (21 blocks for the H–H-type aircraft grid and the C–O-type pylon grids and four blocks for the O–H-type store grids). The number of node points, including the H-type block to improve the domain connection between sub grids, was approximately 2.3 million. The sectional grid system, including the H-type block grid, is shown in Fig. 12. The bomb consisted of four blocks, due to its four tail fins. Three sets of bomb grids were constructed (Table 2), and Fig. 12 shows the medium-grid set. The far-field boundary was extended to 50 times the maximum diameter of the bomb. The steady-state solutions were obtained with 4,000 iterations, with local time stepping for fast convergence. Drag forces and pitching-moment coefficients at various angles of attack were compared with each other; the convergence of the force coefficients is shown in Fig. 13. Based on the grid convergence test, the simulations were carried out with the medium-grid set. Grids for the pylon, the aircraft, and the background flowfield for the overset grids were constructed with a grid resolution based on a medium grid of the bomb in Table 2 for optimal overset regions and computational cost.

The store was released at an altitude of 5,000 ft, with no ejecting force. The freestream Mach number was 0.4, and the aircraft angle of attack was zero. The total computing time for one releasing scenario (from the beginning to approximately 1.1 s) was nearly 8 h, with an unsteady time step of 4.8 ms when using 31 processors of a Linux PC cluster consisting of a Pentium 4 2.6 GHz CPU in each node and linked by a 100 Mbps Ethernet network. The force and moment coefficients are presented in Fig. 14. Relatively small roll moments were generated from the cant angle of the tail fin. The time histories of the incremental coefficients in each scenario are shown in Fig. 15. An incremental coefficient calculation by computation of the aerodynamic forces in the freestream condition was done once for every five unsteady calculations. A total of 49 computations were carried out. The side force and pitching and yawing moments of the inboard case were larger than those of the outboard case, owing to the larger disturbances of the wing and the fuselage. Estimations of the aircraft flowfield effects are tabulated in Table 3. The incremental lift and pitching moment coefficients were initially large. Moreover, different dynamics between the aircraft field and the freestream condition

Table 2 Grid system for generic bomb

Body	No. of blocks	Grid size	Total node points
Coarse	4	$97 \times 13 \times 33$	166,452
Medium	4	$121 \times 17 \times 41$	337,348
Fine	4	$153 \times 25 \times 51$	780,300

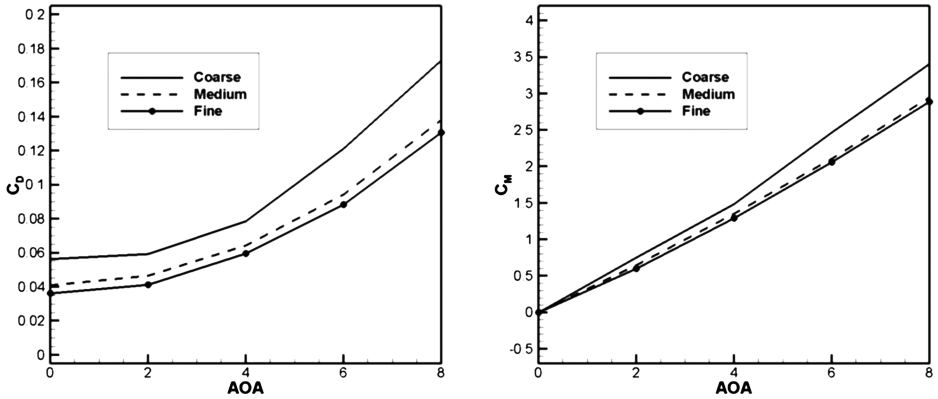

Fig. 13 Drag and pitching moment coefficients of a generic bomb (steady-state solutions).

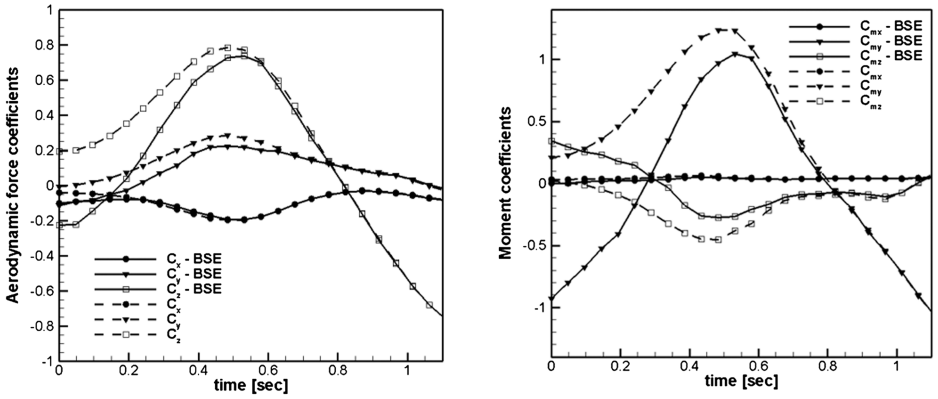

a) Inboard pylon

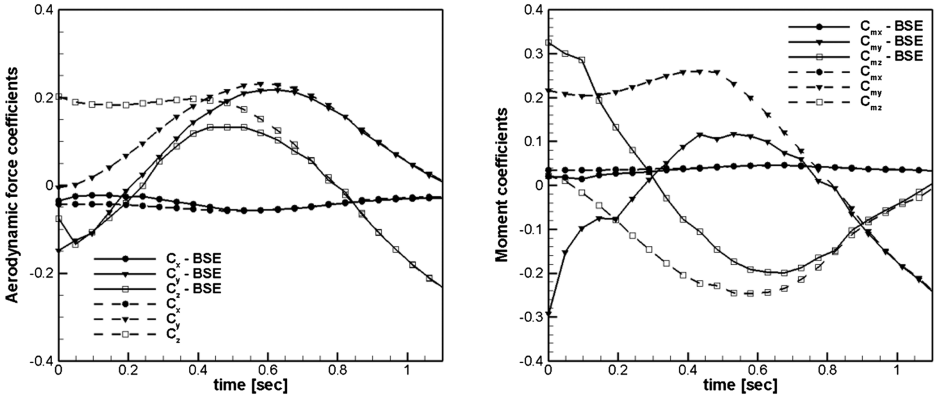

b) Outboard pylon

Fig. 14 Aerodynamic force and moment coefficients (store from aircraft).

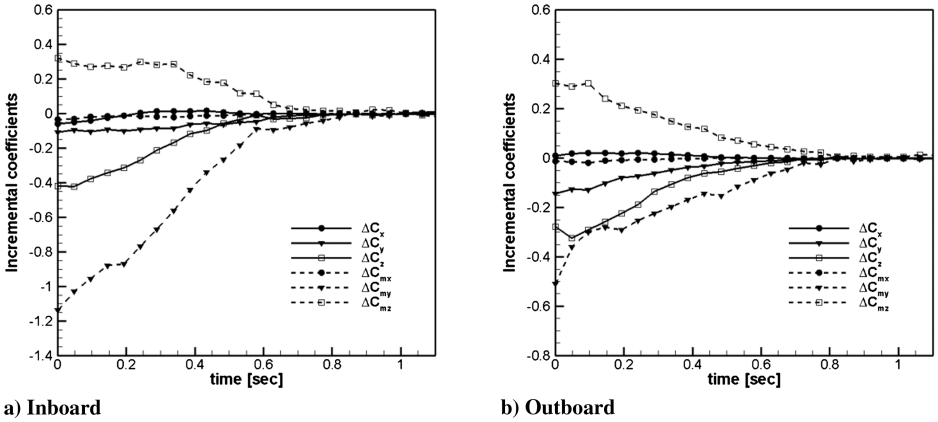

a) Inboard b) Outboard

Fig. 15 Incremental coefficients (store from aircraft).

Table 3 Estimation of the aircraft flowfield

Test case	Diminishing time, s	Lift coefficients (ΔC_z), %	Pitching coefficient (ΔC_{my}), %
Inboard	1.1596	1.22653	0.57368
Outboard	1.1113	0.14575	0.44567

were found in those directions. These large incremental coefficients mostly decayed (below 2% of the maximum values) after 1.1 s. The store departed from the aircraft about 1.52 times the half-span length at this time. Unsteady trajectory calculations up to this time do not require a heavy computing time.

VI. Conclusions

A two-step simulation process can be used for target point estimations and to generate bomb trajectories. In the first step, the released bomb trajectory in the aircraft flowfield was computed. and the BSE was simultaneously checked using the proposed algorithm. Aircraft flowfield effects were calculated directly, without additional computing time, using the parallel computing algorithm. Incremental coefficients were used as an indicator to switch from an unsteady CFD computation in the aircraft flowfield to an offline simulation in the free-flight condition in the second step. The disappearance of the BSE was estimated by means of a direct calculation of the incremental coefficients. Aircraft flowfield effects were counted using this approach.

The accuracy of the flow solver and the grid module, including 6-DOF motion equations, were presented through an application of an Eglin wing/pylon/store case and were subsequently compared with the CTS data. A generic bomb released from a KT-1 aircraft was tested, and the influences of the aircraft flowfield effects were computed. The unsteady time-accurate computation had no interpolation errors, in contrast to a classical method using a database. This makes this method especially suitable for a supersonic or transonic flow with strong nonlinear effects.

The final velocities and the trajectory of the released store presented in this paper were used for the initial conditions of the second step, specifically, the offline simulation of the TGP. The full trajectory to the target points can be predicted accurately with enhanced initial positioning from the present method.

References

[1] Gaton, V. A., and Harmatz, M., "Computational Estimate of the Separation Effect," *Journal of Aircraft*, Vol. 32, No. 6, 1995, pp. 1322–1325.
doi:10.2514/3.46881

[2] Carlson, D. R., King, M. O., and Patterson, R. C., "Integrated Store Separation and Ballistic Accuracy: Applying Enabling Technologies to Improve Aircraft Store Separation," AIAA Paper 1995-3431, Aug. 1995.

[3] Massengill, H. P., Jr., "A Technique for Predicting Aircraft Flow-Field Effects upon an Unguided Bomb Ballistic Trajectory and Comparison with Flight Test Results," AIAA Paper 93-0856, Jan. 1993.

[4] Dillenius, M. F. E., Perkins, S. C., Jr., and Nixon, D., "Pylon Carriage and Separation of Stores," *Tactical Missile Aerodynamics: General Topics*, edited by M. J. Hemsch, Vol. 141, Progress in Astronautics and Aeronautics, AIAA, New York, 1992, pp. 575–666.

[5] Dillenius, M. F. E., Goodwin, F. K., and Nielsen, J. N., "Analytical Prediction of Store Separation Characteristics from Subsonic Aircraft," *Journal of Aircraft*, Vol. 12, No. 10, 1975, pp. 812–818.
doi:10.2514/3.59876

[6] Davids, S., and Cenko, A., "Grid Based Approach to Store Separation," AIAA Paper 2001-2418, June 2001.

[7] Cenko, A., and Waskiewicz, J., "Recent Improvements in Prediction Techniques for Supersonic Weapon Separation," *Journal of Aircraft*, Vol. 20, No. 8, 1983, pp. 659–665.
doi:10.2514/3.44926

[8] Noel, P., Niewoehner, R., and Cenko, A., "Improved Understanding of CFD Predictions for Complex Aircraft/Store Configurations," AIAA Paper 2003-4071, June 2003.

[9] Lijewski, L. E., and Suhs, N. E., "Time-Accurate Computational Fluid Dynamics Approach to Transonic Store Separation Trajectory Prediction," *Journal of Aircraft*, Vol. 31, No. 4, 1994, pp. 886–891.
doi:10.2514/3.46575

[10] Sisco, B., and Cenko, A., "SPLITFLOW Prediction of MK-83 Trajectories from the CF-18 Aircraft," AIAA Paper 2001-2430, June 2001.

[11] Sickles, W. L., Denny, A. G., and Nichols, R. H., "Time-Accurate CFD Predictions of the JDAM Separation from an F-18C Aircraft," AIAA Paper 2000-0796, Jan. 2000.

[12] Steger, J. L., Dougherty, F. C., and Benek, J. A., "A CHIMERA Grid Scheme," *Advances in Grid Generation*, edited by K. N. Ghia, and U. Ghia, ASME-FED-5, American Society of Mechanical Engineers, New York, 1983, pp. 59–69.

[13] Dunworth, K. S., Atkins, D. J., and Lee, J. M., "Incorporation of CFD Generated Aerodynamic Data in Store Separation Predictions," AIAA Paper 2005-846, Jan. 2005.

[14] Kim, E., Park, S. H., and Kwon, J. H., "Parallel Performance Assessment of Moving Body Overset Grid Application on PC Cluster," *Parallel Computational Fluid Dynamics: Parallel Computing and Its Applications*, edited by J. H. Kwon, A. Ecer, J. Periaux, N. Satofuka, and P. Fox, 1st ed., Elsevier, Amsterdam, 2007, pp. 59–66.

[15] Harten, A., "High Resolution Schemes for Hyperbolic Conservation Laws," *Journal of Computational Physics*, Vol. 49, No. 3, 1983, pp. 357–393.
doi:10.1016/0021-9991(83)90136-5

[16] Anderson, W. K., Thomas, J. L., and van Leer, B., "A Comparison of Finite Volume Flux Splittings for the Euler Equations," *AIAA Journal*, Vol. 24, No. 9, 1986, pp. 1453–1460.
doi:10.2514/3.9465

[17] Pulliam, T. H., and Chaussee, D. S., "A Diagonal Form of an Implicit Approximate-Factorization Algorithm," *Journal of Computational Physics*, Vol. 39, No. 2, 1981, pp. 347–363.
doi:10.1016/0021-9991(81)90156-X

[18] Park, S. H., Kim, Y. S., and Kwon, J. H., "Prediction of Damping Coefficients Using the Unsteady Euler Equations," *Journal of Spacecraft and Rockets*, Vol. 40, No. 3, 2003, pp. 356–362.
doi:10.2514/2.3970

[19] Prewitt, N. C., Belk, D. M., and Shyy, W., "Parallel Computing of Overset Grids for Aerodynamic Problems with Moving Objects," *Progress in Aerospace Sciences*, Vol. 36, No. 2, 2000, pp. 117–172.
doi:10.1016/S0376-0421(99)00013-5

[20] Cho, K. W., Kwon, J. H., and Lee, S., "Development of a Fully Systemized Chimera Methodology for Steady/Unsteady Problems," *Journal of Aircraft*, Vol. 36, No. 6, 1999, pp. 973–980.
doi:10.2514/2.2538